American Mineralogist, Volume 80, pages 78–86, 1995

Epitaxial replacement of kyanite by staurolite: A TEM study of the microstructures

Bernardo Cesare
Dipartimento di Mineralogia e Petrologia, Universita di Padova, Corso Garibaldi, 37, 35137 Padua, Italy
Bernard Grobéty*
Institut für Mineralogie und Petrographie, ETH-Zentrum, Sonneggstrasse 5, 8092 Zurich, Switzerland

Abstract

Pelitic schists in the contact aureole of the late-Alpine Vedrette di Ries granodiorite show an epitaxial replacement of kyanite by Fe-rich staurolite. The reaction is observed within nodules of fine-grained staurolite crystals (100–200 μm) containing oriented lamellae of kyanite.

Microprobe, backscattered electron microscopy (BSEM), and high-resolution transmission electron microscopy (HRTEM) investigations demonstrate the presence of submicroscopic intergrowths of staurolite and kyanite. The orientation of both phases, $\mathbf{a}_{St} \| \mathbf{b}_{Ky}$ and $\mathbf{c}_{St} \| \mathbf{c}_{Ky}$, is in agreement with previous observations. Individual staurolite and kyanite lamellae are between one unit cell and some tens of unit cells wide. Detailed observation of the termination of staurolite lamellae within kyanite suggests that the replacement occurs by a solid-state reaction, in which the primary cubic close-packed O framework of kyanite is preserved. The epitaxial replacement implies a reorganization of the site occupancy accompanied by addition of Fe + Mg + H and removal of Si + Al from the reaction site.

The epitaxial replacement of metastable kyanite occurred during contact metamorphism within the andalusite stability field, under temperature and pressure conditions of 500–550 °C and >2.9 kbar, respectively.

Introduction

Staurolite and kyanite are commonly associated in medium-grade pelitic rocks (Deer et al., 1982). Both minerals often occur as epitaxial, macroscopic intergrowths, as in the sample from the Alpe Sponda in the Swiss Alps described by Kenngott (1866, discussed by Wenk, 1980). The close relationship between the structures of both minerals, which contain similar Al_2SiO_5 layers, should facilitate submicroscopic intergrowth of kyanite and staurolite. Wenk (1980) attempted to identify such intergrown sequences of kyanite and staurolite with transmission electron microscopy (TEM), but without success. Fitzpatrick (1976) found minute, isolated regions of kyanite in staurolite samples. These regions are probably the result of the development of nonconservative stacking faults, which lead to the transformation of staurolite to kyanite (Lefebvre, 1982). This paper presents the results of an investigation of staurolite crystals from a contact aureole in the eastern Alps, which show unusual kyanite cores and contain submicroscopic, interfingering lamellae of the two phases.

Geological and petrographic framework

Polymetamorphosed pelitic rocks of the Austridic crystalline basement south of the Tauern Window (eastern Italian Alps) are mainly composed of low-temperature, greenschist-facies, chlorite-muscovite schists, which contain relicts of garnet, fibrous sillimanite, kyanite, and staurolite from earlier metamorphic events. These rocks are the final result of a complex tectono-metamorphic history, characterized by overprinting of greenschist- and amphibolite-facies assemblages of pre-Alpine and Alpine age (Sassi et al., 1974; Bögel et al., 1979; Stöckhert, 1985; Frank et al., 1987). Low-pressure (andalusite + sillimanite + cordierite) contact metamorphism within the aureole of the oligocene Vedrette di Ries granodiorite (Borsi et al., 1979) is the last event recorded in the area; it developed under generally static conditions, with the formation of new biotite, staurolite, andalusite, cordierite, sillimanite, garnet and potassium feldspar, following the prograde sequence described by Cesare (1992).

The mica schists in which staurolite replaces kyanite are exposed at the southern border of the granodiorite (Mager, 1985). They form a well-defined layer 30 m thick about 1 km from the intrusion, within the andalusite + staurolite zone of contact metamorphism (zones as defined by Cesare, 1992). In this zone, the schists are characterized by orange-brown nodular aggregates of staurolite (maximum diameter of 5–6 mm), which sometimes preserve a garnet core. A second layer of similar rock type is exposed closer to the intrusive contact (600 m). This layer is also within the andalusite + staurolite zone. The temperatures, slightly higher compared with the first layer, resulted in a coarsening of both single crystals and

* Present address: Department of Earth and Planetary Sciences, Johns Hopkins University, Baltimore, Maryland 21218, U.S.A.

0003–004X/95/0102–0078$02.00

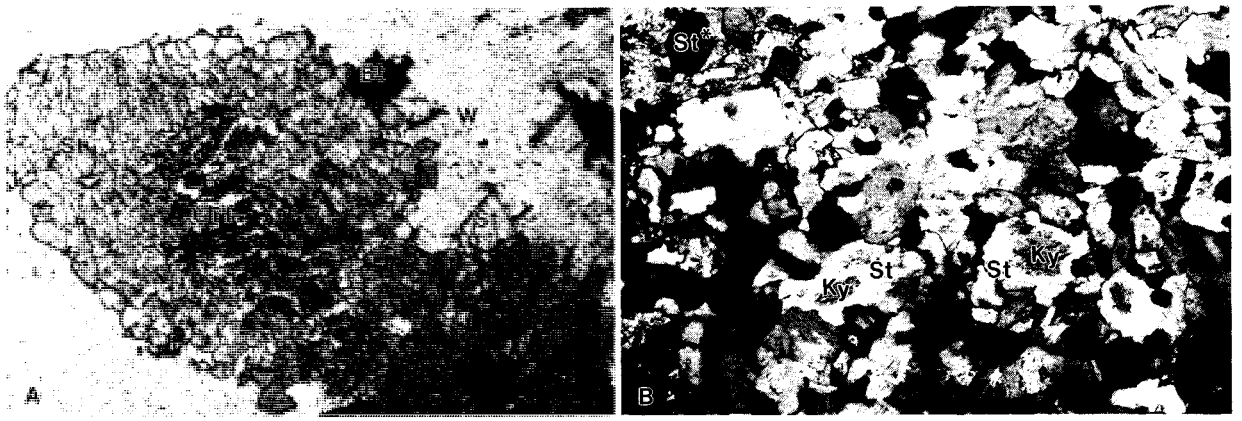

Fig. 1. (A) Photomicrograph of a nodular aggregate of staurolite (St), with garnet relicts (Grt) in the core. Staurolite grows within a sericitic white mica patch (W), together with newly formed biotite (Bt). Note the euhedral shape of staurolite at the edge of the cluster. (Plane-polarized light, width of photo 2.5 mm.) (B) Close-up photomicrograph of a staurolite nodule. Kyanite cores (Ky) within staurolite display higher birefringence. The staurolite at the edge (St*) is optically homogeneous. (Crossed polars, width of photo 0.8 mm.)

nodules. The stable assemblage related to contact metamorphism in the schists with nodular aggregates of staurolite consists of quartz, plagioclase, biotite, chlorite, muscovite (and fine-grained sericite), staurolite, andalusite, ilmenite, and graphite.

Staurolite, which formed during the contact event, appears either as isolated, euhedral crystals or as polycrystalline aggregates within sericite-rich patches (Fig. 1A). The aggregates correspond to the macroscopically visible nodules. The staurolite crystals in the nodules are very fine-grained and randomly oriented; the grain size and degree of idiomorphism increase toward the edge of nodules, where crystals could grow without impinging on each other. Although these textures developed within a primary garnet site (Cesare, 1991), staurolite does not seem to replace garnet directly.

In detail, staurolite crystals within nodules show optical discontinuities, and their colorless cores exhibit higher birefringence, no pleochroism, and the presence of cleavage, typical of kyanite (Fig. 1B). Heterogeneities generally are present in the grains of the central part of the nodule, whereas edge crystals are optically homogeneous. These microstructures were investigated by BSEM and HRTEM techniques.

Table 1. Microprobe analyses of staurolite and kyanite

	Staurolite		Kyanite	Optically homogeneous staurolite*		
Sample	VR491	VR498	VR491	VR491a	VR491b	VR491c
No. of analyses	7	30	4			
SiO_2	28.19(0.33)	27.23(0.46)	37.12(0.25)	35.55	35.39	30.67
TiO_2	0.49(0.07)	0.50(0.12)	0.05(0.06)	0.03	0.22	0.35
Al_2O_3	54.75(0.37)	55.32(0.53)	63.07(0.23)	60.58	60.33	56.69
FeO_{tot}**	12.87(0.24)	13.05(0.40)	0.27(0.07)	2.94	4.46	10.43
MnO	0.10(0.01)	0.10(0.03)	0.00 —	0.01	0.01	0.13
MgO	1.05(0.13)	1.41(0.21)	0.00 —	0.13	0.35	0.11
ZnO	0.26(0.07)	0.15(0.07)	0.00 —	n.a.	n.a.	n.a.
H_2O	2.17(0.02)	2.17(0.00)				
Total	99.92(0.70)	99.95(0.40)	100.55(0.08)	99.25	100.77	99.38
	Number of ions on the basis of 48 (O,OH) for staurolite and 5 (O,OH) for kyanite					
Si	7.785(0.041)	7.533(0.138)	0.997(0.006)			
Ti	0.103(0.015)	0.103(0.024)	0.001(0.001)			
Al	17.822(0.102)	18.049(0.165)	1.997(0.008)			
Fe	2.973(0.047)	3.020(0.101)	0.005(0.002)			
Mn	0.024(0.003)	0.023(0.007)	— —			
Mg	0.429(0.052)	0.572(0.094)	— —			
Zn	0.054(0.015)	0.031(0.015)	— —			
OH	4.000	4.000				
X_{Fe}†	0.85–0.89	0.82–0.89				

Note: mean values of analyses are given; standard deviation = 1σ.

* Contains submicroscopic kyanite lamellae.

** Total Fe considered as Fe^{2+} in staurolite and Fe^{3+} in kyanite (Deer et al., 1982).

† $X_{Fe} = Fe_{tot}/(Fe_{tot} + Mg)$.

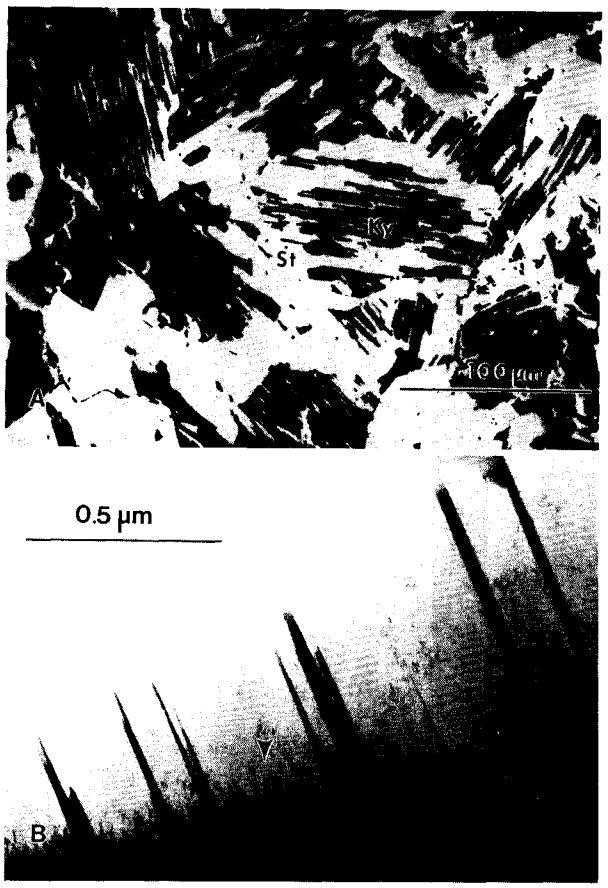

Fig. 2. (A) Backscattered electron image showing the kyanite + staurolite intergrowth. A decussate aggregate of grains composed of kyanite relicts (dark) forming patches and lamellae within staurolite (bright). (B) Low-magnification bright-field image of staurolite lamellae (dark spikes) within kyanite. The mottled contrast of kyanite (arrow) is due to incipient beam damage.

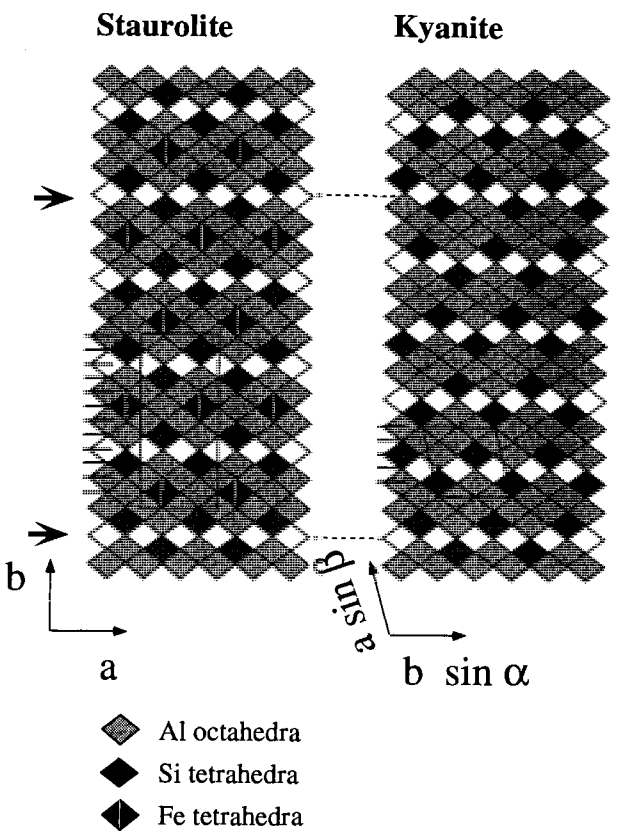

Fig. 3. Schematic c axis projection of the kyanite and staurolite structures (modified after Wenk, 1980). Arrows indicate (quasi-)coherent interlayers of empty channels in both structures (3% mismatch). The level of the anions within the unit cells (outlined) are indicated by short lines on the left side.

KYANITE + STAUROLITE INTERGROWTH

Experimental techniques

Two samples with the textures described above were analyzed by wavelength-dispersive spectrometry with a Cameca SX50 electron microprobe. A 15-kV accelerating voltage, 20-nA beam current, 1-μm beam diameter, and a counting time of 10 s were used for each element. Natural and synthetic silicates and oxides were used as standards. Matrix effects were corrected using a PAP-enhanced ZAF correction method (Pouchon and Pichoir, 1984).

Two samples were prepared for TEM observations. The 3-mm ion-milled and C-coated disks were mounted on a 30° double-tilt holder. The electron microscopy was performed with a JEOL 200 CX, having spherical aberration C_S = 2.8 mm, focus spread = 11 nm, and point to point resolution of 0.3 nm. HRTEM photographs were obtained at an accelerating potential of 200 kV using objective apertures 40 and 70 μm in diameter, centered on the central beam at conditions close to the Scherzer defocus value.

One difficulty encountered was the instability of kyanite under electron radiation. Amorphization of the kyanite structure along the foil edges occurred within seconds. Most pictures were therefore taken in thicker parts of the foil. Image simulations were made using the multislice method (HRTEM simulation program package EMS, Stadelmann, 1987). Structural data for kyanite and staurolite for the simulation were taken from Winter and Ghose (1979) and Smith (1968), respectively.

Mineral chemistry

The average chemical compositions of kyanite and staurolite, obtained from single points and profiles across homogeneous grains, are listed in Table 1. Kyanite is almost pure Al_2SiO_5, with 0.2–0.3 wt% Fe_2O_3. The Fe^{3+} content in kyanite is similar to that of the stable andalusite that occurs in the same specimen; the latter may, however, contain up to 1 wt% Fe_2O_3 in pink pleochroic cores. Staurolite is Fe-rich and weakly zoned with respect to Fe-Mg, as indicated by the low standard deviations in Table 1 and restricted range of X_{Fe}. The mean compositions of staurolite in all the analyzed samples are very

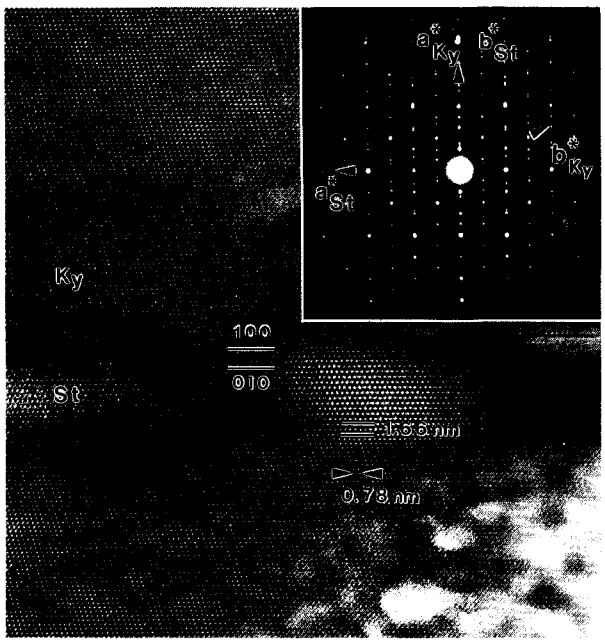

Fig. 4. HRTEM image of a coherent staurolite (St) lamella seven unit cells wide within kyanite (Ky). The indicated spacings correspond to the *b*-cell parameters of both structures. No stacking faults are present close to the interface. Insert: corresponding selected-area electron diffraction (SAED) pattern. No streaking, kyanite superstructure, or twin reflections (Wenk, 1980) are present.

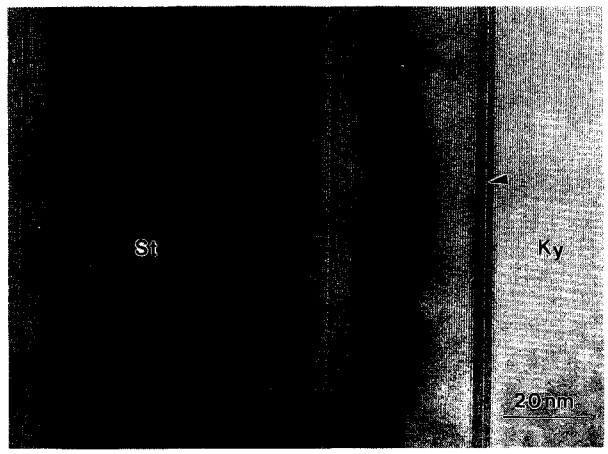

Fig. 5. A [001] image of an intergrowth of kyanite (Ky) (light) and staurolite (St) (dark) lamellae. The rightmost staurolite lamella contains a single kyanite layer (arrow). On both sides of the large staurolite lamella are single staurolite layers within kyanite.

similar, and the only systematic chemical variation is the slight decrease of X_{Fe} (also observed in coexisting chlorite) in samples where kyanite replacement is closer to completion (VR498 compared with VR491). The higher ZnO concentration in the staurolite-poor sample (VR491) is consistent with the inverse correlation between Zn content and the modal abundance of staurolite suggested by Guidotti (1970) and Tuisku et al. (1987).

Although staurolite compositions listed in Table 1 are very close to those of grains from the matrix outside the nodules, they should be interpreted with caution. In fact, several analyses of optically homogeneous parts of the staurolites gave mixed compositions (analyses VR491a, VR491b, and VR491c in Table 1), which are inconsistent with both ferrian aluminium silicate (see Kerrick, 1990, p. 19) and staurolite stoichiometries. The origin of the mixed compositions is revealed by BSE and low-magnification TEM images (Fig. 2A, 2B), which show the presence of intimately interfingered kyanite and staurolite lamellae. High-resolution transmission electron microscopy (HRTEM) was used to investigate the nature and the origin of these intergrowths.

HRTEM

The kyanite and staurolite structures are closely related. Kyanite contains chains of edge-sharing AlO_6 octahedra parallel to [001]. These chains form slabs parallel to $(100)_{Ky}$, which are interconnected by isolated SiO_4 tetrahedra and additional AlO_6 octahedra. The connecting planes are characterized by empty octahedra (Fig. 3). Staurolite contains similar Al_2SiO_5 units, but with an additional monolayer of approximate composition $^{[4]}Al_{0.7}{}^{[4]}Fe_2O_2(OH)_2$ between each kyanite unit (Ribbe, 1982). Both structures can also be described as slightly distorted cubic close-packed arrays of O atoms with different occupancies of the octahedral and tetrahedral sites.

The similarity of the two structures results in oriented, macroscopic parallel intergrowths between both phases, which are often observed in rocks where kyanite coexists with or replaces staurolite (and vice versa). The orientation relationship is given by $\mathbf{a}_{St} \| \mathbf{b}_{Ky}$ and $\mathbf{c}_{St} \| \mathbf{c}_{Ky}$.

The almost perfect compatibility of the $(010)_{St}$ and $(100)_{Ky}$ planes theoretically permits the stacking of layers of both structures perpendicular to these planes in any combination. Previous electron diffraction studies of the specimens from Alpe Sponda in the Swiss Alps, where oriented kyanite and staurolite coexist, revealed no submicroscopic intergrowth (Wenk, 1980). The interfaces were characterized only by an increase of defects (stacking faults and twins) in kyanite close to the boundary and generally defect-free staurolite.

In the present samples, interlayering on the scale of the unit cell of both phases is common (Fig. 4). Interlayering is predominantly present in the transition zone between the staurolite rims and the kyanite-rich cores of grains in the centers of the nodules (see Fig. 2A). The widths of the lamellae range from one unit cell up to several tens of unit cells. In the samples studied, closely spaced single staurolite layers in kyanite and vice versa are rare (Fig. 5). No ordered mixed-layer sequences were detected. Odd and even numbers of unit layers within lamellae are equally observed, and the numbers are not multiples of each other.

Both kyanite and staurolite lamellae contain stacking faults. The dominant defects found in kyanite were (100)

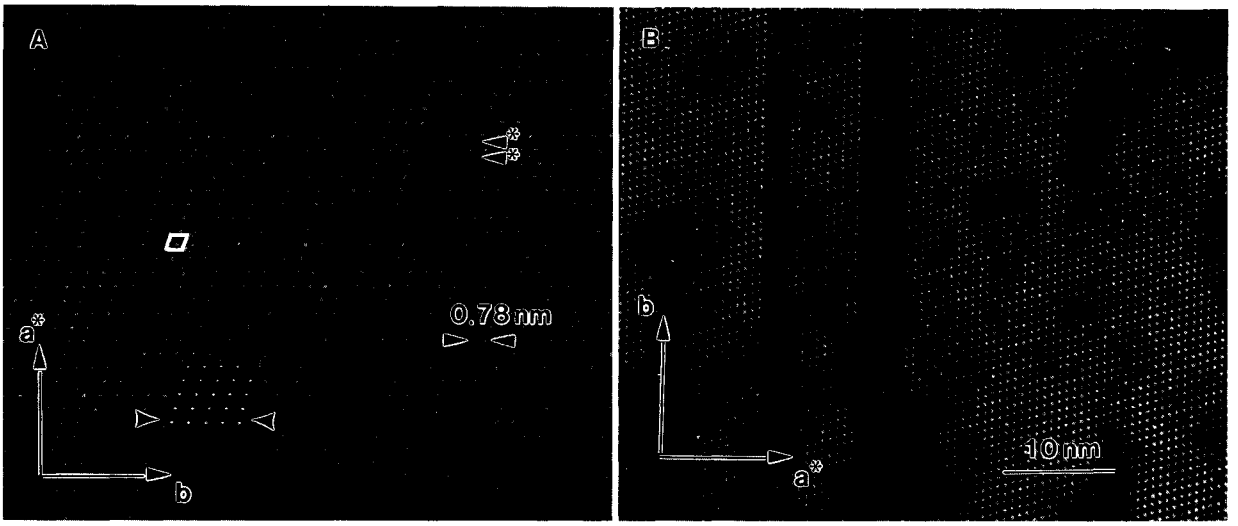

Fig. 6. (**A**) HRTEM image of kyanite. The lower left insert is a calculated image for a thickness of 20 nm at Scherzer focus. The arrows on both sides of the insert indicate the position of the plane with the empty octahedral channels. The two arrows marked by asterisks indicate stacking faults. (**B**) Two γ microtwins in kyanite.

stacking faults with a ½ [010] displacement vector. Two types of planar stacking faults related to the (100)[001] slip system in kyanite are known. The full displacement vectors of these faults are ½ [001] and ½ [011]. Both are associated with the dissociation of the [001] perfect dislocation in kyanite (Lefebvre and Menard, 1981). The ½ [010] slip component observed for the stacking faults in the present specimens (Fig. 6A) suggests that they belong to the second type. The γ microtwins (Fig. 6B) result from the periodic introduction of such stacking faults. In kyanite growing on staurolite, as in the Alpe Sponda sample studied by Wenk (1980), such faults occur preferentially

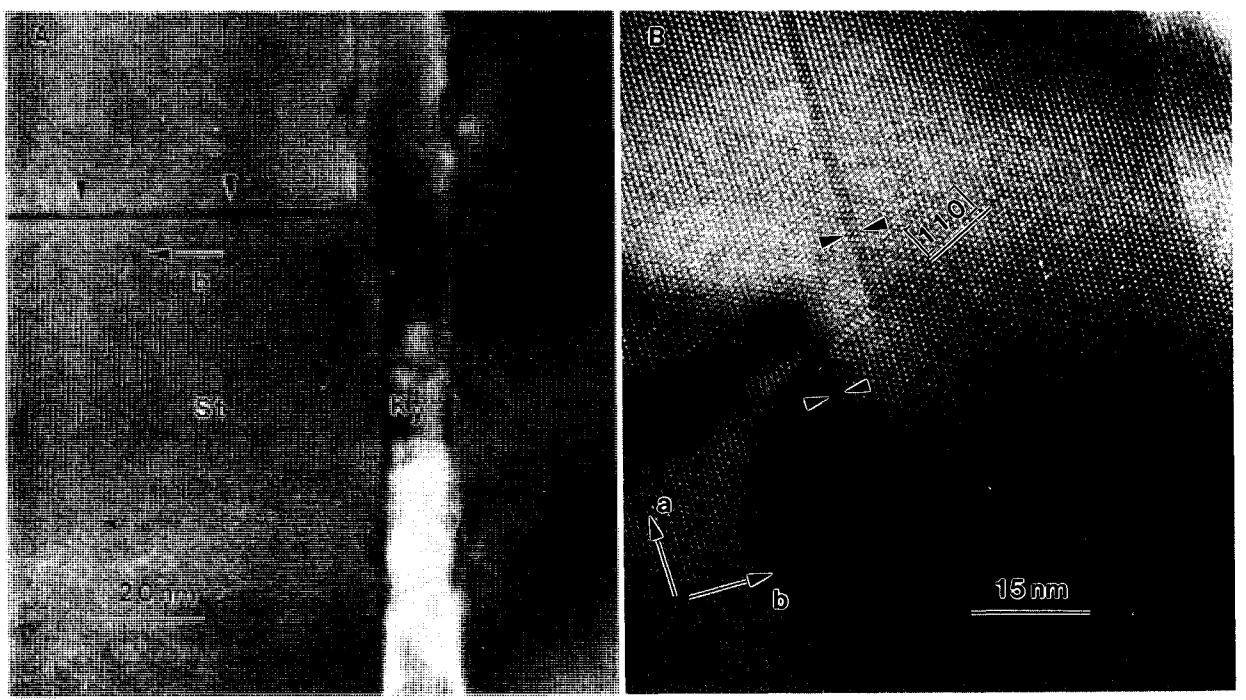

Fig. 7. (**A**) A [001] image of a kyanite (Ky) lamella in staurolite (St). The irregular width is due to growth ledges of staurolite along both interfaces. The dark line (arrows) represents a stacking fault starting from the tip of the growth ledge. The visible displacement is ¼ [010] (**B**) Triple kyanite layer in staurolite connected through a stacking fault running along [110] with a double kyanite layer. The dark contrast on the left of the stacking fault is due to a dislocation within kyanite.

in the vicinity of the interface. They are therefore considered to reflect the different stacking order of the Al_2SiO_5 units within staurolite after the removal of the hydroxide (=OH) layers and should be observed in kyanite that is replacing staurolite (Lefebvre, 1982). In the present samples the faults and microtwins occur throughout the kyanite core and are not related only to the $(010)_{St}$-$(100)_{Ky}$ interface.

Rare stacking faults, parallel to $(010)_{St}$ or $(110)_{St}$, were observed within the otherwise defect-poor staurolite lamellae. They start from growth ledges on the boundary of kyanite lamellae (Fig. 7A) or from isolated kyanite within staurolite (Fig. 7B). They compensate for the missing OH layers in the kyanite layers (Fig. 7B). The full displacement vectors have not yet been clearly identified.

The terminations of staurolite lamellae within the kyanite core are not bound to a particular lattice plane, as they are for the $(010)_{St}$-$(010)_{Ky}$ interface (Fig. 8). The ends of broad lamellae are often corrugated, giving rise to irregular moiré patterns. Within the O substructures, there is a considerable mismatch between $\mathbf{b}_{St}$ and $\mathbf{a}^*_{Ky}$, the corresponding direction in the kyanite structure. This mismatch is due to the extra OH layers in staurolite. The interatomic distances between different O atoms within these OH layers are considerably larger then the equivalent distances in the kyanite-like part of the staurolite structure. Along $\mathbf{b}_{St}$ are 12 O layers; along $\mathbf{a}^*_{Ky}$ are five O layers per unit cell. Knowing the lattice parameters of both phases from diffraction patterns of the [001] zone (see insert in Fig. 4: 1.665 nm for b_{St} and 0.715 nm for a_{Ky}) we can calculate the average distance between the individual O layers: $b_{St}/12 = 0.138$ nm, $a^*_{Ky}/5 = a \sin \beta \cos(\gamma - 90°)/5 = 0.134$ nm. The periodicity at which the empty interlayers in both structures are approximately coherent (3.33 nm vs. 3.35 nm) is five layers in kyanite along the **a*** direction, which corresponds to four layers in staurolite along the **b** direction (see arrows in Fig. 3). The resulting average mismatch of the O substructure along this direction between the two structures is, therefore, on the order of 0.6%. Along the common **c** axis, the misfit is approximately 1.5%, and the smallest difference is recorded along $\mathbf{a}_{St} \| \mathbf{b}_{Ky}$ (0.2%). This (quasi-)coherency is characterized by lattice fringes that pass straight through the boundary (Fig. 9). For the conditions under which Figure 9 was taken, these fringes coincide with the plane containing the row of empty octahedra. It should be noticed that only the empty interlayer is coherent, but the site occupancy in the corresponding Al_2SiO_5 units may be different in the two minerals. The other rows, both in staurolite and kyanite, show no bending and end at the boundary. The boundary itself is sharp and contains several steps.

Another typical feature of the lamella termination in Figure 9 is the array of bright spots situated on the kyanite side of the interface. A similar feature can be seen at the termination of a staurolite slab that is a unit cell thick (Fig. 10A). The bright spot (lower right insert Fig. 10A) deviates slightly from the regular position of the white

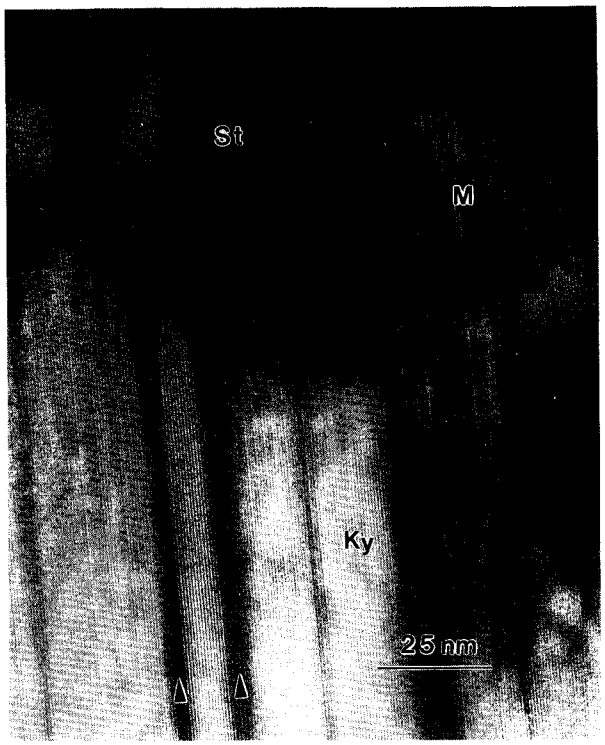

Fig. 8. A [001] image of a termination of a broad staurolite (St) lamella in kyanite (Ky). Some narrow staurolite lamellae start from this interface. The terminations of staurolite lamellae are not restricted to a specific lattice plane. The corrugated interface gives rise to moiré patterns (M).

dots that are characteristic of the contrast of the surrounding kyanite. Figure 10B shows the most likely atomic configuration around the termination shown in Figure 10A. The kyanite layers at the top and at the bottom of the staurolite slab are continuous. The lower layer of empty octahedral channels in the staurolite slab is displaced by approximately one octahedral layer compared with the same layer in the matrix kyanite. This leads to an unusual accumulation of octahedral channels at the boundary (see outlined box in Fig. 10B). To test the influence of such an accumulation of channels on the contrast of HRTEM pictures, image simulations were performed using the EMS program (Stadelmann, 1987). The defect, an extra column of empty octahedra replacing a regular column of AlO_6 octahedra, was embedded in a 4 × 4 × 1 supercell of kyanite. The multislice calculations were performed using the periodic continuation method (Wilson and Spargo, 1982). The supercell was cut into two slices perpendicular to the beam. All beams passing through a 4-nm^{-1} aperture were included in the image calculations. Simulations for different thicknesses, focus settings, and positions of the extra channel were performed. Despite the great simplification of ignoring the presence of the nearby boundary with staurolite, a good match between the experimental image and the calculated contrast (arrow in the lower right insert in Fig. 10A)

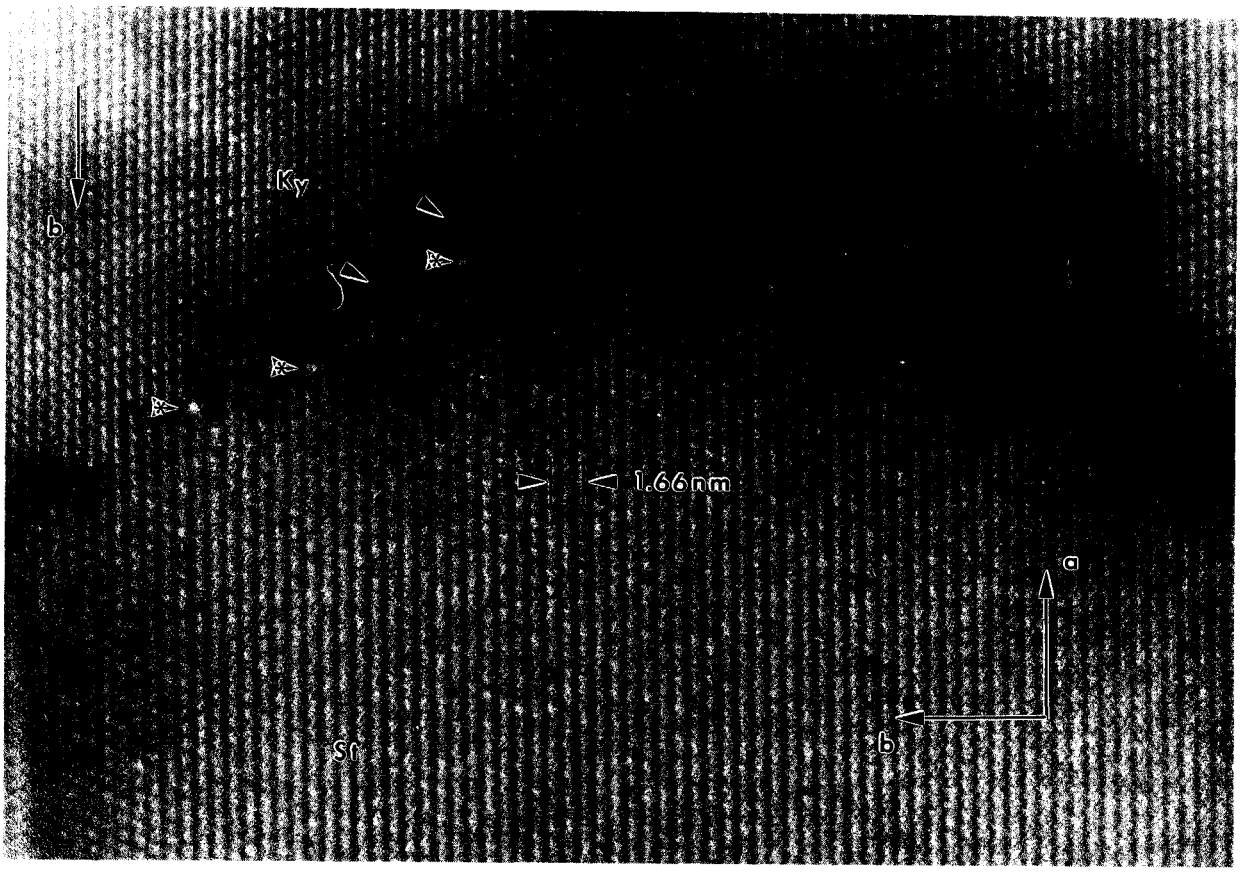

Fig. 9. Staurolite (St) lamella termination in kyanite (Ky). The right part of the boundary is shadowed, probably because of the presence of mechanical stresses caused by the slight misfit between the O substructures of both structures. The arrows indicate boundary crossing lattice fringes. They are separated by six fringes in kyanite and five in staurolite. The arrows marked by asterisks point to bright spots, which probably represent unusual arrangements of empty octahedral channels at the interface.

was achieved for an empty column in the position shown in Figure 10B.

The first kyanite layer below the staurolite slab in the proposed atomic arrangement (Fig. 10B) is incomplete. Two layers of octahedra are missing, and the separation of the two layers of empty octahedra is, therefore, reduced to 0.4 nm compared with the normal value of 0.67 nm. A reduction of the first fringe spacing below the staurolite slab can, indeed, be observed in the experimental image.

The replacement of kyanite by staurolite

The analyzed intergrowth of kyanite and staurolite may indicate either equilibrium coexistence (Chinner, 1961; Deer et al., 1982, p. 344) or replacement. An origin of the second kind for the studied structures and the assessment of kyanite and staurolite as reactant and product phase, respectively, are texturally constrained in two ways. First, the nodules occur in schists where andalusite is the stable Al_2SiO_5 polymorph and where microstructural evidence indicates a synchronous growth of andalusite and staurolite; second, samples from outcrops at variable distances from the intrusion show an increasing degree of kyanite replacement with increasing metamorphic grade (Cesare, 1992).

The absence of transition regions at the terminations of staurolite lamellae and the boundary-crossing lattice fringes suggest continuity of at least a part of the primary kyanite structure. For the replacement of staurolite by kyanite, Lefebvre (1982) proposed the elimination of the entire OH layer as a possible reaction mechanism, on the basis of the observation of nonconservative stacking faults in staurolite. This mechanism preserves the Al_2SiO_5 layers and requires a volume decrease of 25%. For the replacement of kyanite by staurolite, the introduction of an entire OH layer would result in a volume increase of the same amount. The generally observed macroscopic texture—for example, the reaction proceeding from the rim to the center of kyanite—resulting in the complete mantling by staurolite, can hardly be reconciled with a 25% volume increase.

The preservation of the O substructure of kyanite during the replacement would imply a volume increase of only about 3% and a slight displacive reorganization of

the anions, due to the different distortion of the O substructure in staurolite. Given a constant O framework, and using the staurolite and kyanite compositions of sample VR498 (Table 1), we would find the resulting reaction stoichiometry at the interface: $48Al_2SiO_5 + 2.8Mg + 15.1Fe + 0.5Ti + 20H + 0.1Mn + 0.25Zn \rightarrow 5Mg_{0.56}Fe_{3.02}Zn_{0.05}Mn_{0.02}Al_{18.05}Ti_{0.1}Si_{7.53}O_{44}(OH)_4 + 5.75Al + 10.35Si$.

A complete reorganization of the site occupancy within the cubic close-packed array of O atoms at the phase boundary, the net removal of Si + Al, and the net addition of Fe + Mg + H and minor Zn + Ti + Mn are the consequences of the proposed reaction mechanism. The nucleation happens not only at the interface between core and rim, but also within the kyanite core (Fig. 10A). Similar mechanisms are described in oxide systems, for example, in the reaction couple $NiO\text{-}NiAl_2O_4\text{-}Al_2O_3$ (Schmalzried, 1978). The phase boundary reaction consists essentially of a redistribution of ions in the interstices of the O substructure. At the first interface of the above reaction couple, the O substructure is perfectly coherent, but at the second the coherency is only partial, and the hexagonal close-packed O ions in alumina must be transformed through partial dislocations into the face-centered cubic structure of the O in the spinel phase.

The decrease of X_{Fe} in coexisting staurolite and chlorite and the textural observations on mineral abundance variations suggest that the Fe, Mg, and H required for staurolite formation are supplied by dissolving chlorite, possibly along AFM continuous equilibria (Thompson and Norton, 1968; Thompson, 1976), in which biotite and muscovite are also involved. Metastable, relict garnet is also a likely reactant. The Al and Si released by the reaction are probably used for the simultaneous formation of andalusite and quartz in the matrix.

Loss and gain of elements from staurolite aggregates require mass-transport mechanisms effective on the dimension of the staurolite rim. The empty octahedral sites forming the open channels parallel to $[001]_{Ky}$ were probably important as an easy diffusion path and as an intermediate site during the reorganization. Depending on the progress of the cation reorganization, different site occupancies and arrangements of channels can occur (see Fig. 10A). The bright spots along the termination represent such clustering of channels. The isolated stacking faults and twins in kyanite are probably caused by mechanical stresses that are connected with the slight volume increase connected with the reaction.

The discussed epitaxial replacement of kyanite by staurolite occurred as a metastable reaction within the andalusite stability field during contact metamorphism. Pressure and temperature conditions during this solid-state reaction were determined using cation-exchange and solid-solid thermobarometry and by comparison of observed assemblages with published and calculated petrogenetic grids in the KFMASH system (Cesare, 1992). The estimated values of temperature and pressure are 500–550 °C and >2.9 kbar, respectively.

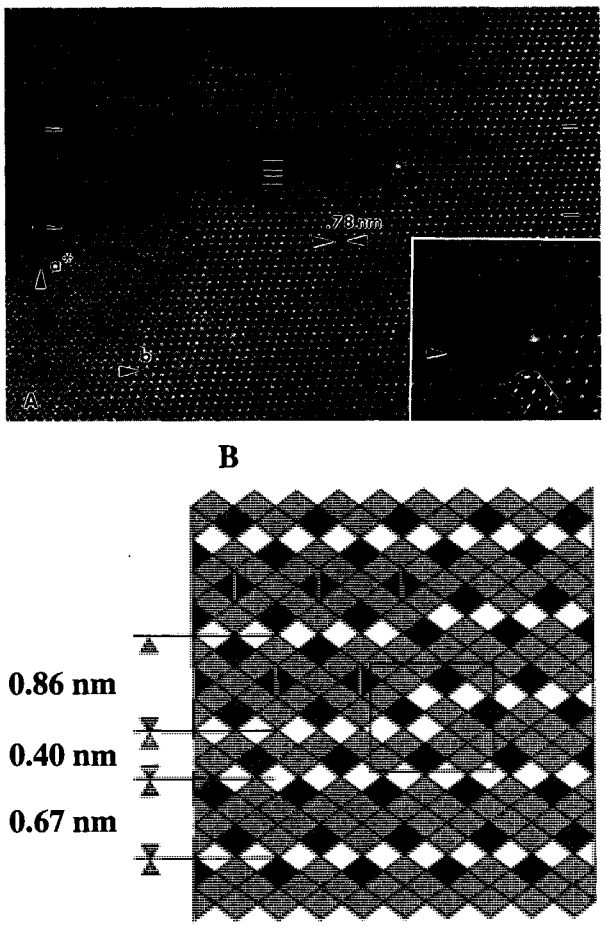

Fig. 10. (**A**) A [001] image of a staurolite nucleus within kyanite. The first fringe distance below the staurolite layer is reduced and represents an incomplete kyanite layer. The slight bending of the arrowed lattice row is due to the different dimension of the O substructure in staurolite, causing a slight volume increase. The black lines (left and right side of the picture) indicate identical lattice planes. The left side of the staurolite layer has one more kyanite layer between these lines than the right side. The staurolite therefore originates at a dislocation within kyanite. The lower right insert shows a magnification of the right staurolite termination. A simulated image (thickness 22 nm at Scherzer focus) of the defect outlined in **B** is inserted below the termination. (**B**) Schematic interpretation of the site occupancies around the right staurolite termination. The polyhedra of the OH layers in staurolite have the same size as those of the kyanite layers. The outlined box shows the unusual clustering of empty octahedra, which leads to the unusual contrast shown in **A**.

ACKNOWLEDGMENTS

This research was initiated when B.C. was a guest at the Institut für Mineralogie und Petrographie of the ETH, Zurich, with the financial support of the Italian Consiglio Nazionale delle Ricerche (MURST 40%) and Schweizerischer Nationalfonds (grant 831-031398), as well as Fondazione Gini (Padua). Analytical facilities were provided by the Centro di Studio per i Problemi dell'Orogeno Alpi Orientali (C.N.R., Padua), the Labor für Elektronenmikroskopie, ETH, Zurich, and the Institut für Mineralogie und Petrographie, ETH, Zurich.

We would like to thank C.V. Guidotti, J. Connolly, and D. Veblen, for critical reading of an early version of the manuscript, and reviewers for their helpful comments.

REFERENCES CITED

Bögel, H., Morteani, G., Sassi, F.P., Satir, M., and Schmidt, K. (1979) The Hercynian and pre-Hercynian development of the eastern Alps. Neues Jahrbuch der Geologischen und Paläontologischen Gesellschaft Abhandlungen, 159, 87–112.

Borsi, S., Del Moro, A., Sassi, F.P., and Zirpoli, G. (1979) On the age of the Vedrette di Ries (Rieserferner) massif and its geodynamic significance. Geologische Rundschau, 68, 41–60.

Cesare, B. (1991) Polyphase microstructural evolution of a primary garnet site: An example from the Vedrette di Ries contact aureole (eastern Alps, Italy). Plinius (supplement to European Journal of Mineralogy), 6, 130.

——— (1992) Metamorfismo di contatto di rocce pelitiche nell'aureola di Vedrette di Ries (Alpi Orientali, Italia). Ph.D. dissertation, University of Padua, Padua, Italy.

Chinner, G.A. (1961) The origin of sillimanite at Glen Cova, Angus. Journal of Petrology, 2, 312–323.

Deer, W.A., Howie, R.A., and Zussman, J. (1982) Staurolite. In Rock-forming minerals, vol. 1A: Orthosilicates (2nd edition), p. 817–866. Longman, London.

Fitzpatrick, J.J. (1976) Studies in the microstructure and crystal chemistry of minerals. Ph.D. dissertation, University of California, Berkeley, California.

Frank, W., Kralik, M., Scharbert, S., and Thöni, M. (1987) Geochronological data from the eastern Alps. In H.W. Flugel and P. Faupl, Eds., Geodynamics of the eastern Alps, p. 272–281. Deuticke, Vienna.

Guidotti, C.V. (1970) The mineralogy and petrology of the transition from the lower to upper sillimanite zone in the Oquossoc area, Maine. Journal of Petrology, 11, 277–336.

Kenngott, A. (1866) Die Minerale der Schweiz, 135 p. Englemann, Leipzig, Germany.

Kerrick, D.M. (1990) The Al_2SiO_5 polymorphs. In Mineralogical Society of America Reviews in Mineralogy, 22, 360 p.

Lefebvre, A. (1982) Lattice defects in three structurally related minerals: Kyanite, yoderite and staurolite. Physics and Chemistry of Minerals, 8, 251–256.

Lefebvre, A., and Menard, D. (1981) Stacking faults and twins in kyanite, Al_2SiO_5. Acta Crystallographica, A37, 80–84.

Mager, D. (1985) Geologische Karte der Rieserfernergruppe zwischen Magerstein und Windschar (Sudtirol). Der Schlern, 6, 22 p.

Pouchon, J.L., and Pichoir, F. (1984) Un nouveau modèle de calcul pour la microanalise quantitative par spectrométrie de rayon-X: I. Application à l'analyse d'échantillons homogènes. La Recherche Aérospatiale, 3, 167–192.

Ribbe, P.H. (1982) Aluminum silicate polymorphs and mullite. In Mineralogical Society of America Reviews in Mineralogy, 5, 189–214.

Sassi, F.P., Zanferrari, A., Zirpoli, G., Borsi, S., and Del Moro, A. (1974) The Austrides to the south of the Tauern Window and the Periadriatic Lineament between Mules and Mauthen. Neues Jahrbuch der Geologischen und Paläontologischen Gesellschaft Monatshefte, 7, 421–439.

Schmalzried, H. (1978) Reactivity and point defects of double oxides with emphasis on simple silicates. Physics and Chemistry of Minerals, 2, 279–294.

Smith, J.V. (1968) The crystal structure of staurolite. American Mineralogist, 53, 1139–1155.

Stadelmann, P.A. (1987) EMS: A software package for electron diffraction analysis and HREM image simulation in material science. Ultramicroscopy, 21, 131–146.

Stöckhert, B. (1985) Pre-Alpine history of the Austridic basement to the south of the western Tauern window (Southern Tirol, Italy): Caledonian versus Hercynian event. Neues Jahrbuch der Geologischen und Paläontologischen Gesellschaft, Monatshefte, 10, 618–642.

Thompson, A.B. (1976) Mineral reactions in pelitic rocks: I. Prediction of *P-T-X* (Fe-Mg) phase relations. American Journal of Science, 276, 401–424.

Thompson, J.B., and Norton, S.A. (1968) Paleozoic regional metamorphism in New England and adjacent areas. In E-an Zen, Ed., Studies of Appalachian geology: Northern and maritime, p. 319–327. Interscience, New York.

Tuisku, P., Ruostesuo, P., and Häkkinen, A. (1987) The metamorphic behaviour and petrogenetic significance of zinc in amphibolite facies, staurolite-bearing mica schists, Puolankajärvi Formation, central Finland. Geochimica et Cosmochimica Acta, 51, 1639–1650.

Wenk, H.R. (1980) Defects along kyanite-staurolite interfaces. American Mineralogist, 65, 766–769.

Wilson, A.R., and Spargo, A.E.C. (1982) Calculation of the scattering from defects using periodic continuation methods. Philosophical Magazine, Series A 46, 435–445.

Winter, J.K., and Ghose, S. (1979) Thermal expansion and high-temperature crystal chemistry of the Al_2SiO_5 polymorphs. American Mineralogist, 64, 573–586.

MANUSCRIPT RECEIVED APRIL 20, 1994
MANUSCRIPT ACCEPTED SEPTEMBER 26, 1994